

Single-event-transient effect in nanotube tunnel field-effect transistor with bias-induced electron-hole bilayer

Xue-Ke Wang(王雪珂), Ya-Bin Sun(孙亚宾), Zi-Yu Liu(刘子玉), Yun Liu(刘赟), Xiao-Jin Li(李小进), and Yan-Ling Shi(石艳玲)

Citation: Chin. Phys. B, 2023, 32 (**6**): 064209. DOI: 10.1088/1674-1056/ac9180
Journal homepage: http://cpb.iphy.ac.cn; http://iopscience.iop.org/cpb

What follows is a list of articles you may be interested in

Research on the model of high robustness computational optical imaging system

Yun Su(苏云), Teli Xi(席特立), and Xiaopeng Shao(邵晓鹏)
Chin. Phys. B, 2023, 32 (**2**): 024202. DOI: 10.1088/1674-1056/ac9b34

A radiation-temperature coupling model of the optical fiber attenuation spectrum in the Ge/P co-doped fiber

Yong Li(李勇), Haoshi Zhang(张浩石), Xiaowei Wang(王晓伟), and Jing Jin(金靖)
Chin. Phys. B, 2022, 31 (**7**): 074211. DOI: 10.1088/1674-1056/ac40f9

Loss prediction of three-level amplified spontaneous emission sources in radiation environment

Shen Tan(谭深), Yan Li(李彦), Hao-Shi Zhang(张浩石), Xiao-Wei Wang(王晓伟), and Jing Jin(金靖)
Chin. Phys. B, 2022, 31 (**6**): 064211. DOI: 10.1088/1674-1056/ac43a8

Temperature-responded tunable metalenses based on phase transition materials

Jing-Jun Wu(伍景军), Feng Tang(唐烽), Jun Ma(马骏), Bing Han(韩冰), Cong Wei(魏聪), Qing-Zhi Li(李青芝), Jun Chen(陈骏), Ning Zhang(张宁), Xin Ye(叶鑫), Wan-Guo Zheng(郑万国)‡, and Ri-Hong Zhu(朱日宏)
Chin. Phys. B, 2022, 31 (**5**): 054216. DOI: 10.1088/1674-1056/ac3cad

Irradiation study of liquid crystal variable retarder for Full-disk Magneto-Graph payload onboard ASO-S mission

Jun-Feng Hou(侯俊峰), Hai-Feng Wang(王海峰), Gang Wang(王刚), Yong-Quan Luo(骆永全), Hong-Wei Li(李宏伟), Zhen-Long Zhang(张振龙), Dong-Guang Wang(王东光), Yuan-Yong Deng(邓元勇)
Chin. Phys. B, 2020, 29 (**7**): 074208. DOI: 10.1088/1674-1056/ab8c40

Single-event-transient effect in nanotube tunnel field-effect transistor with bias-induced electron–hole bilayer

Xue-Ke Wang(王雪珂)[1], Ya-Bin Sun(孙亚宾)[1,†], Zi-Yu Liu(刘子玉)[2,‡], Yun Liu(刘赟)[1], Xiao-Jin Li(李小进)[1], and Yan-Ling Shi(石艳玲)[1]

[1] *Department of Electrical Engineering, East China Normal University, Shanghai* 200241, *China*
[2] *School of Microelectronics, Fudan University, Shanghai* 200433, *China*

(Received 25 April 2022; revised manuscript received 6 September 2022; accepted manuscript online 13 September 2022)

The single event transient (SET) effect in nanotube tunneling field-effect transistor with bias-induced electron–hole bilayer (EHBNT-TFET) is investigated by 3-D TCAD simulation for the first time. The effects of linear energy transfer (LET), characteristic radius, strike angle, electrode bias and hit location on SET response are evaluated in detail. The simulation results show that the peak value of transient drain current is up to 0.08 mA for heavy ion irradiation with characteristic radius of 50 nm and LET of 10 MeV·cm^2/mg, which is much higher than the on-state current of EHBNT-TFET. The SET response of EHBNT-TFET presents an obvious dependence on LET, strike angle, drain bias and hit location. As LET increases from 2 MeV·cm^2/mg to 10 MeV·cm^2/mg, the peak drain current increases monotonically from 0.015 mA to 0.08 mA. The strike angle has an greater impact on peak drain current especially for the smaller characteristic radius. The peak drain current and collected charge increase by 0.014 mA and 0.06 fC, respectively, as the drain bias increases from 0.1 V to 0.9 V. Whether from the horizontal or the vertical direction, the most sensitive hit location is related to w_t. The underlying physical mechanism is explored and discussed.

Keywords: heavy ion strike, EHBNT-TFET, single event transient (SET), transient drain current

PACS: 42.88.+h, 85.30.Mn **DOI:** 10.1088/1674-1056/ac9180

1. Introduction

Integrated circuits develop towards low power consumption in the era of the Internet-of-things (IOT). Limited by the lowest sub-threshold slope (*SS*) of 60 mV/decade at room temperature, it is not feasible for conventional MOSFETs to reduce the power consumption only by lowering the supply voltage.[1] Taking the advantage of band-to-band tunneling (BTBT), tunneling field effect transistor (TFET) promises *SS* less than 60 mV/dec and improves the short-channel performance.[2,3] However, TFET suffers from low on-state current (I_{ON}) and low experimental *SS*.[4,5] Several architectures have been explored to improve the performance of TFET, such as double gate TFET,[6] L-shaped TFET (LTFET),[7] gate-all-around arch-shaped TFET,[8] nanotube TFET with a core source (CSNT-TFET),[9] and electron–hole bilayer TFET (EHBTFET).[10] In our recent work, an intentional misaligned inner-gate and outer-gate is adopted in electron–hole bilayer nanotube TFET (EHBNT-TFET), and an improved I_{ON} and ultra-steep *SS* are obtained.[11]

Low power devices have shown great attraction in the space electronic systems. In space radiation environment, cosmic rays and solar electromagnetic radiation bring the unfavorable single-event-transient (SET) effect, resulting in increased probability of soft-error, reliability degradation, function abnormal and even failure of semiconductor devices and circuits.[12–14] It is meaningful to analyze the SET effect on TFETs, so as to evaluate the potential of TFETs for space applications. Abundant literatures on SET effect are available for MOSFETs and MOSFET-based circuits.[15–18] Recently, research about SET effect in TFET has been studied. Manohari *et al.*[19] evaluated the SET of three types TFET, including traditional planar TFET, pocket-based planar TFET and LTFET. The results showed that LTFET has a better radiation performance. However, their research only focused on the comparison between three types TFET, and the physical mechanism was not discussed in their work. Wu and Takahashi[20] discussed heavy-ion-induced transient in conventional MOSFET and TFET. It was observed that TFET can eliminate the parasitic bipolar effects. Wang *et al.*[21] studied SET effect in LTFET and fully depleted silicon on insulator (FDSOI). They found that LTFET is more sensitive to SET than FDSOI and the tunneling junction in LTFET is the most sensitive region. Chong *et al.*[22] proposed that SET-sensitive region in T-shaped TFET and LTFET is tunneling junction because both of the devices are vertical TFETs. However, the above literatures focus on 2-D TFET structures, and few researches are documented on the radiation performance in 3-D electron–hole bilayer TFET.

In this work, the single-event-transient (SET) effect in EHBNT-TFET is evaluated by using 3-D TCAD simulation for the first time. The result shows that a significant SET cur-

†Corresponding author. E-mail: ybsun@ee.ecnu.edu.cn
‡Corresponding author. E-mail: liuziyu@fudan.edu.cn

© 2023 Chinese Physical Society and IOP Publishing Ltd

rent which is much larger than the on-state current occurs in EHBNT-TFET for heavy ion irradiation. The linear energy transfer, strike angle, drain bias and hit location is found to have a great impact on SET response. This paper is organized as follows. The device structure and simulation methodology are presented in Section 2. The effects of linear energy transfer, characteristic radius, strike angle, electrode bias and hit location on SET response are discussed in Section 3. The conclusion is drawn in Section 4.

2. Device structure and simulation methodology

Figure 1 presents the investigated EHBNT-TFET. The inner-gate and outer-gate oxide is composed of 2.82 nm HfO_2, and the isolation is filled with SiO_2. The doping concentration in p-type source and n-type drain is separately 5×10^{19} cm^{-3} and 1×10^{18} cm^{-3}. The channel is intrinsic silicon. The channel thickness is 5 nm, and the inner-gate and outer-gate work-function are separately 5.4 eV and 3.8 eV. The key structure parameters are listed in Table 1. Sentaurus TCAD software is used to evaluate the performance of EHBNT-TFET.[23] Besides the conventional recombination and mobility model, the dynamic nonlocal BTBT model and density gradient (DG) model taking into account quantum confinement effect are included.

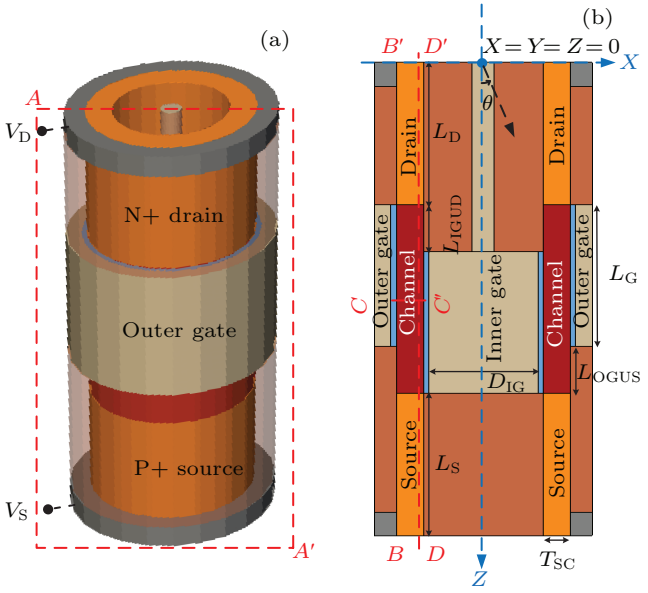


Fig. 1. Structure of the EHBNT-TFET investigated in this work: (a) 3-D schematic view and (b) cross-sectional view along A–A' cut-plane.

The simulation environment is firstly calibrated by reproducing the result of NT-TFET in Ref. [24]. As plotted in Fig. 2(a), the simulated transfer curve shows a good agreement with the data in Ref. [24], which proves the validity of our simulation environment. In addition, DG model has been also calibrated on the solution of Poisson–Schrödinger equation. The parameters are given as follows: $\gamma_n = 7$, $\gamma_p = 10.5$, $\eta_n = 1.02$, $\eta_p = 0.8$, $\theta_n = 0.91$ and $\theta_p = 0.97$. As shown in Fig. 2(b), charge distributions over channel for calibrated DG model matches well with Schrödinger equation.

Table 1. Device parameters used for the simulations.

Parameters	EHBNT-TFET
Inner-gate diameter (D_{IG})	80 nm
Silicon channel thickness (T_{SC})	5 nm
Gate length (L_G)	30 nm
Source length (L_S)	10 nm
Drain length (L_D)	10 nm
Underlap between inner-gate and drain (L_{IGUD})	10 nm
Underlap between outer-gate and source (L_{OGUS})	10 nm
Inner-gate work-function (Φ_{IG})	5.4 eV
Outer-gate work-function (Φ_{OG})	3.8 eV

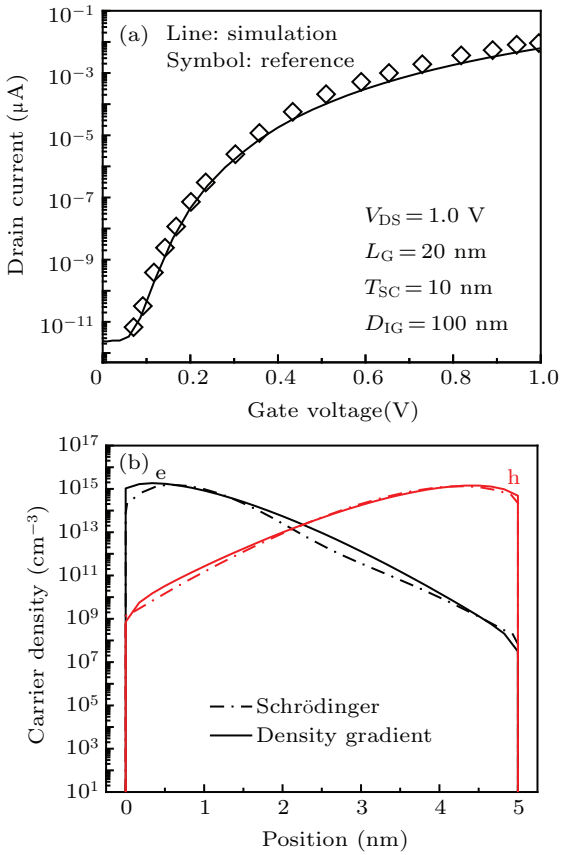


Fig. 2. (a) Validation of the simulation environments by reproducing the transfer characteristic curve of Ref. [24]. (b) Carrier density distributions along C–C' cut-line arising from calibrated DG model and Schrödinger results for EHBNT-TFET.

The asymmetric bias and work-function configuration of the inner-gate (IG) and outer-gate (OG) leads to the formation of electron–hole bilayer in the thin silicon nanotube channel. Thus, the line tunneling takes place inside the channel, realizing improved I_{ON} and low SS, as depicted in Fig. 3. The ratio of I_{ON}/I_{OFF} is found to be 1.5×10^9. Furthermore, EHBNT-TFET exhibits a sub-60 mV/dec SS for seven orders of magnitude of drain current, and the minimum SS is 1.7 mV/dec, as observed in Fig. 3(b).

SET in EHBNT-TFET is evaluated by activating the heavy ion model in Sentaurus tool. When heavy ion strikes

the semiconductor device, a significant number of electron–hole pairs (EHPs) are produced along the incident path. The generation rate of EHPs is calculated as[23,25,26]

$$G(l,w,t) = G_{\mathrm{LET}}(l)R(w)T(t), \tag{1}$$

$$G_{\mathrm{LET}}(l) = \frac{1}{\pi w_{\mathrm{t}}^2}\mathrm{LET_}f(l), \tag{2}$$

$$R(w) = \mathrm{e}^{-w^2/w_{\mathrm{t}}^2}, \tag{3}$$

where l, w and t are separately the length, radius and strike time of heavy ion track. $G_{\mathrm{LET}}(l)$ is the LET generation density, describing the generated charge per length along the ion track. $R(w)$ and $T(t)$ take into account the spatial and temporal gaussian distribution functions of the generation rate. w_{t} is characteristic radius of heavy ion and $\mathrm{LET_}f(l)$ is linear energy transfer (LET). In our simulation, the time distribution centered on 20 ps with a characteristic width of 2 ps, and track length is set as 100 nm. A characteristic radius of 50 nm and LET of 10 MeV· cm^2/mg is used (unless otherwise specified). The LET value is kept constant along the track.

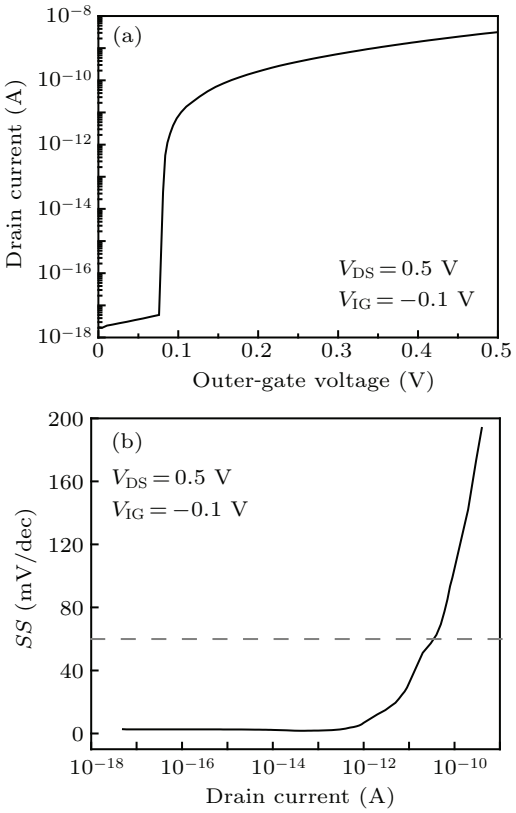


Fig. 3. (a) Transfer characteristic curve and (b) SS of EHBNT-TFET under $V_{\mathrm{DS}} = 0.5$ V.

3. Results and discussion

3.1. Heavy-ion-induced transient in EHBNT-TFET

Considering the vertical symmetric structure of EHBNT-TFET, the ion strikes at the center of the device ($X = 0$, $Y = 0$, $Z = 0$) and the incidence direction is parallel to the channel (along the z-axis), as shown in Fig. 1(b). Figure 4 depicts the variation of transient drain current (I_{d}) and the corresponding collected charge (Q_{coll}) with different LETs under on-state ($V_{\mathrm{DS}} = 0.5$ V, $V_{\mathrm{IG}} = -0.1$ V, and $V_{\mathrm{OG}} = 0.5$ V). Here, I_{d} has removed the contribution of steady-state current before the ion strike. Q_{coll} is derived by integrating I_{d} over the transient duration. Apparently, transient drain current rises up to a peak after heavy ion enters into the device and then diminishes drastically. At the same time, the collected charge saturates quickly. As LET increases from 2 MeV·cm^2/mg to 10 MeV·cm^2/mg, the peak drain current ($I_{\mathrm{d_peak}}$) rises up monotonically from 0.015 mA to 0.08 mA, which is much larger than the on-state current of 0.012 μA/μm. An approximately linear increase of Q_{coll} from 0.082 fC to 0.413 fC is observed, respectively.

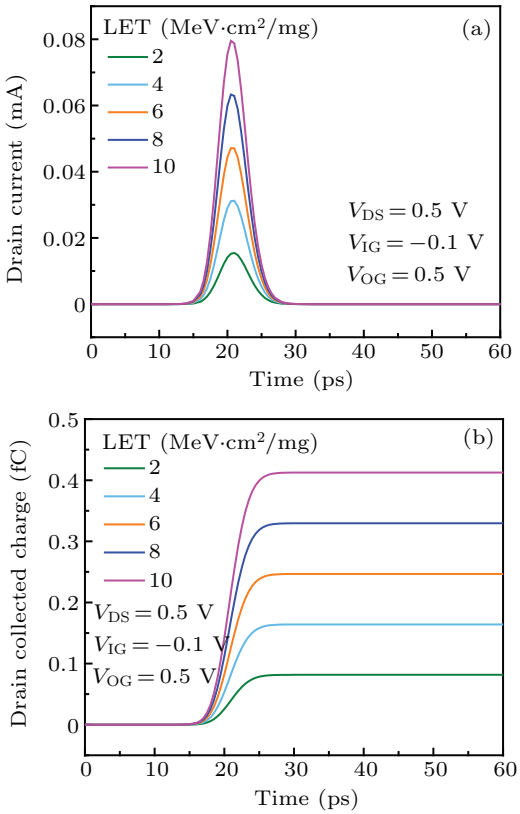


Fig. 4. (a) Transient drain current and (b) collected charge after heavy ion strike with various LETs under on-state.

The formation of above transient current is ascribed the charge collection of the device electrodes through drift-diffusion mechanism. Due to the asymmetrical source/drain doping in EHBNT-TFET, the energy band from drain to source shows a stepwise increasing trend, as reported in Fig. 5(a). Therefore, the generated electrons and holes along the ion track are separately collected by drain and source. The bipolar gain effect and additional charge collection in conventional MOSFET is obvious due to hole accumulation in the channel,[21,27,28] which is negligible in EHBNT-TFET owing to ambipolar transport. In addition, part of EHPs recombines in the charge collection process. Therefore, the carrier density decreases rapidly, leading to a short transient drain current tail.

When the heavy ion strikes the device in normal incidence, amount of charge will be generated in semiconductor. The density of heavy ion-generated charge is shown in Fig. 5(b). The ion track region along the track axis (z-axis) can be defined by track length and track radius. The charge density induced by heavy ion irradiation decreases away from track axis, as depicted in Fig. 5(b). The electron density before and after the ion strike is plotted in Fig. 5(c). These figures indicate that electron density is strongly enhanced after the ion strike (for $t = 20$ ps) and then decreases until it returns to the initial state, because the generated electrons are collected or recombined. With LET of incident particles increasing, more EHPs are generated with a larger LET value and then collected by the drain, leading to larger $I_{\text{d_peak}}$ and Q_{coll}.

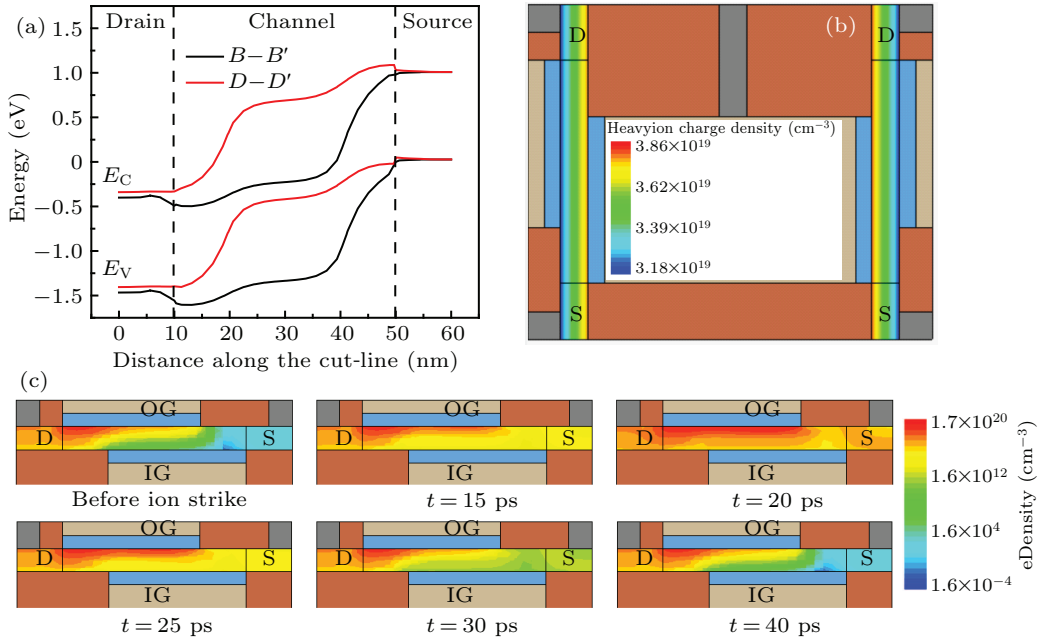


Fig. 5. (a) Energy band diagrams along B–B' cut-line and D–D' cut-line under on-state before ion strike. 2-D profile in A–A' cross section of (b) heavy ion-generated charge and (c) electron over time under on-state when the ion strikes the device in normal incidence, LET = 10 MeV·cm^2/mg, $w_t = 50$ nm.

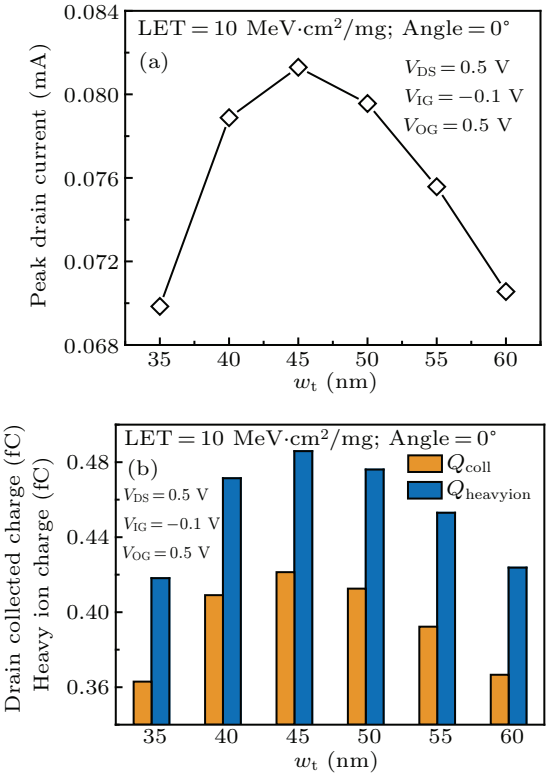


Fig. 6. (a) Peak drain current and (b) the corresponding collected charge and heavy ion-generated charge for several characteristic radius.

The effect of characteristic radius (w_t) is investigated, as depicted in Fig. 6. Here the incidence position is fixed at $X = Y = Z = 0$ and the direction is along the z-axis. LET is at 10 MeV·cm^2/mg and the transistor operates under on-state. The peak drain current and integrated collected charge are found to increase firstly as w_t ranges from 35 nm to 45 nm, then gradually drop with w_t rising up to 65 nm. The charge density induced by heavy ion irradiation is proportional to $G_{\text{LET}}(l)$ and $R(w)$. Heavy ion-generated charge (Q_{heavyion}) is the integration of the charge density over the semiconductor region in EHBNT-TFET. Owing to Gaussian spatial distribution, Q_{heavyion} reaches the maximum at $w_t = 45$ nm, as illustrated in Fig. 6(b). Because the track axis is in the center of EHBNT-TFET, when w_t is lower than 45 nm, the majority of heavy ion-generated charge is located within the inner-gate region, and little Q_{heavyion} generates over silicon nanotube. As w_t increases to 45 nm, the ion track region gradually arrived in the channel, so that more Q_{heavyion} could strike the silicon nanotube. The increased peak current and collected charge is expected with w_t increasing. However, when w_t is larger than 45 nm, part of Q_{heavyion} locates outside the nanotube. Therefore, Q_{heavyion} within the silicon nanotube decreases as w_t increases, resulting in the reduced peak drain current and collected charge.

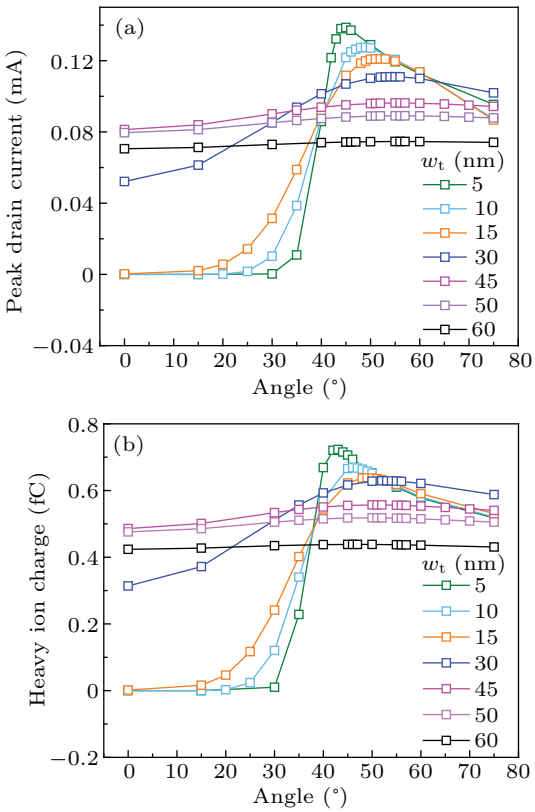


Fig. 7. (a) Peak drain current and (b) the corresponding heavy ion-generated charge for several angles under on-state with various w_t, LET = 10 MeV·cm^2/mg.

Figure 7 depicts the impact of the ion strike angle (θ) considering different w_t, and the incidence position is fixed at $X = Y = Z = 0$. The strike angle θ is defined as the angle between the ion incidence direction and the z-axis. I_{d_peak} and $Q_{heavyion}$ increase firstly and then decrease with θ increasing. As w_t increases, the variation trend of I_{d_peak} and $Q_{heavyion}$ gradually slow down. The distribution of heavy ion-generated charge is concentrated about the track axis under small w_t, so that $Q_{heavyion}$ changes drastically with θ varying. However, $Q_{heavyion}$ remains nearly unchanged under large w_t. Therefore, I_{d_peak} presents a similar trend as $Q_{heavyion}$. As presented in Fig. 8, the strike angle for the maximum I_{d_peak} increases monotonously from 45° to 56° when w_t increases to 35 nm, and then keeps unchanged when w_t further increases, i.e., the maximum of I_{d_peak} appears when the track axis passes through the region near the center of channel. The strike angle for the maximum $Q_{heavyion}$ increases firstly and then declines, which reaches a maximum of 53° at $w_t = 30$ nm. In addition, the strike angle corresponding to the maximum of I_{d_peak} is always greater than that of $Q_{heavyion}$. The difference in θ corresponding to the maximum of I_{d_peak} and $Q_{heavyion}$ is attributed to the decreased recombination when the ion strikes with larger θ. With strike angle increasing, the track axis along strike angle gradually passes through the source region, and then moves to the channel and drain. Correspondingly, the electron–hole pairs begin to appear toward drain side. Less electrons are recombined in collection path, leading to a larger SET current. I_{d_peak} is mainly affected by $Q_{heavyion}$ when w_t is lower than 30 nm, so that θ corresponding to the maximum of I_{d_peak} and $Q_{heavyion}$ has the same increasing trend with w_t increasing. When w_t exceeds 30 nm, the electron collection path has greater effect on I_{d_peak} and the maximum of I_{d_peak} appears at $\theta = 56°$, where the track axis passes through the region near the center of channel. SET current is not only related to the heavy ion-generated charge in the device, but also the distance from the hit location to drain.

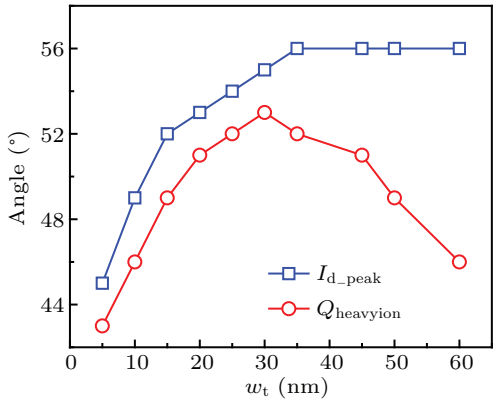


Fig. 8. The strike angle corresponding to the maximum of peak drain current and heavy ion-generated charge with various w_t.

3.2. Impact of bias conditions on SET in EHBNT-TFET

The effect of drain bias on SET response for EHBNT-TFET is studied in Fig. 9. The peak drain current and collected charge present an upward trend with V_{DS} increasing. As V_{DS} increases from 0.1 V to 0.9 V, peak drain current charge increases 0.014 mA and 0.06 fC respectively. Figure 9(b) presents the SRH recombination rate, Auger recombination rate and impact ionization rate in the silicon nanotube region at $t = 20$ ps. The sum of SRH recombination rate and Auger recombination rate decreases with V_{DS} increasing. On the contrary, the impact ionization rate increases monotonously, resulting in more carriers generated in the channel. The declined recombination rate and increased impact ionization rate contribute to a more severe SET current. To understand the mechanism further, we evaluated the 1-D profile of electric field along D–D' cut-line at $t = 20$ ps after the ion strike. In EHBNT-TFET, high electric field is located in the channel and the electric field in source/drain is relatively low, as illustrated in Fig. 9(c). Generally, SRH recombination mainly occurs in the weak electric field region (source/drain), and impact ionization takes place at the strong electric field region (channel). Auger recombination mainly is located at high carrier density region, i.e., source region and the channel near outer-gate, which is consistent with the profile in Fig. 9(d). The electric field in drain and channel region becomes larger with higher V_{DS}. When electric field in drain is enhanced, the velocity of carrier drifting toward the drain end increases and

then electron density in the channel near outer-gate decreases, weakening the SRH and Auger recombination. Besides, larger electric field in the channel results in the acceleration of carrier motion, leading to higher impact ionization rate. Therefore, a worse SET effect is expected under high V_{DS}.

Meanwhile, the impact of outer-gate bias is investigated in Fig. 10. As V_{OG} ranges from 0.1 V to 0.9 V, the peak drain current decreases 0.04 mA. The electric field in the channel increases and electric field in drain reduces as V_{OG} increases, as plotted in Fig. 10(b). The higher electric field in the channel leads to larger impact ionization rate. However, as V_{OG} gradually increases, more electrons are induced in the channel near outer-gate, resulting in increased Auger recombination rate. In addition, SRH recombination becomes larger owing to declined electric field in drain. Under the opposite influence of recombination and impact ionization, I_{d_peak} decreases slightly with V_{OG} increasing.

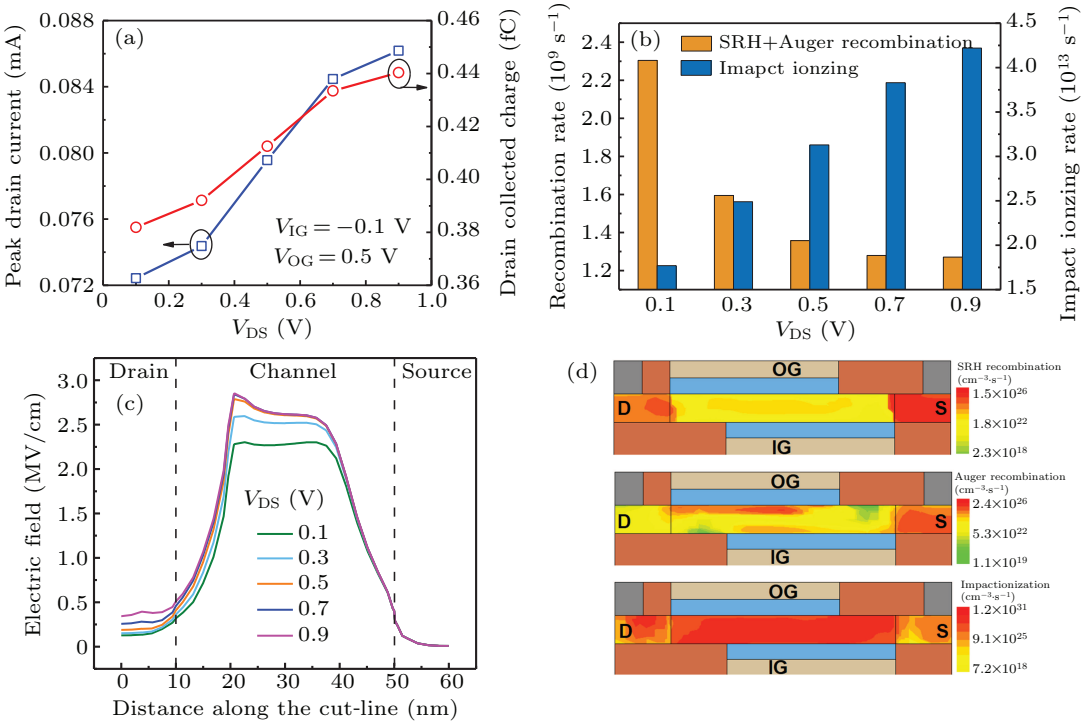


Fig. 9. (a) Peak drain current and collected charge with various V_{DS}. At $t = 20$ ps, (b) recombination rate and impact ionization rate and (c) electric field curves along D–D' cut-line with various V_{DS}; (d) the 2-D profile of SRH recombination, Auger recombination and impact ionization in A–A' cross section at $V_{DS} = 0.5$ V.

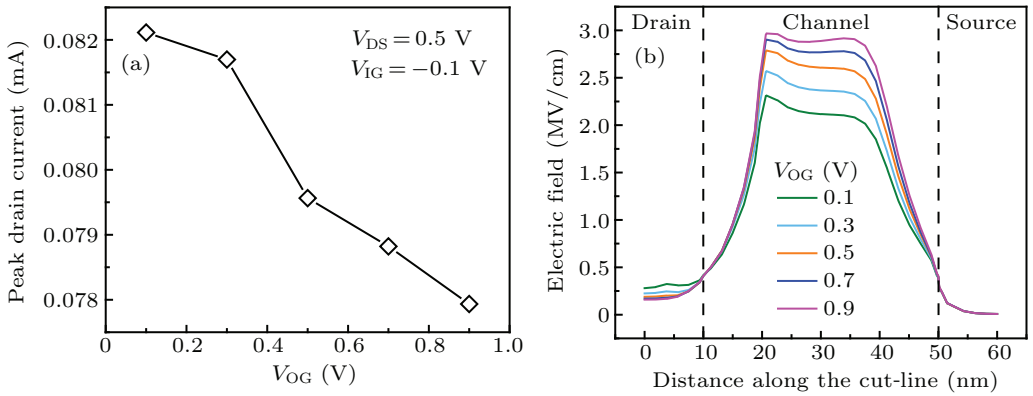


Fig. 10. (a) Peak drain current and (b) electric field curves along D–D' cut-line at $t = 20$ ps with various V_{OG}.

3.3. Heavy ion hit location sensitivity

As heavy ion could strike the device at any direction, we explore the hit location sensitivity from the vertical and horizontal directions. The peak drain current and heavy ion-generated charge at several vertical hit locations with various w_t is plotted in Fig. 11. When w_t is lower than 30 nm, I_{d_peak} increases firstly and then goes down, when the hit location moves from the inner-gate contact (V1) to the outside of silicon nanotube (V5), and the maximum value appears at V4. When w_t exceeds 30 nm, I_{d_peak} declines slightly when hit location moves from V1 to V5. A similar trend of heavy ion-generated charge is presented in Fig. 11(c). The ion track

region is small under w_t of 5 nm, so that heavy ion-generated charge strikes the silicon only at hit location near the channel (V4). As w_t increases to 30 nm, $Q_{heavyion}$ gradually increases at location away from V4 due to larger ion track region, which shows an opposite trend at V4. When w_t exceeds 30 nm, because of the larger ion track region and cylinder structure of nanotube, the heavy ion-generated charge could act on silicon at V1. Heavy ion-generated charge locates in silicon nanotube reduces when strike position is close to the edge of EHBNT-TFET. Less EHPs are generated in the device, leading to reduced I_{d_peak}.

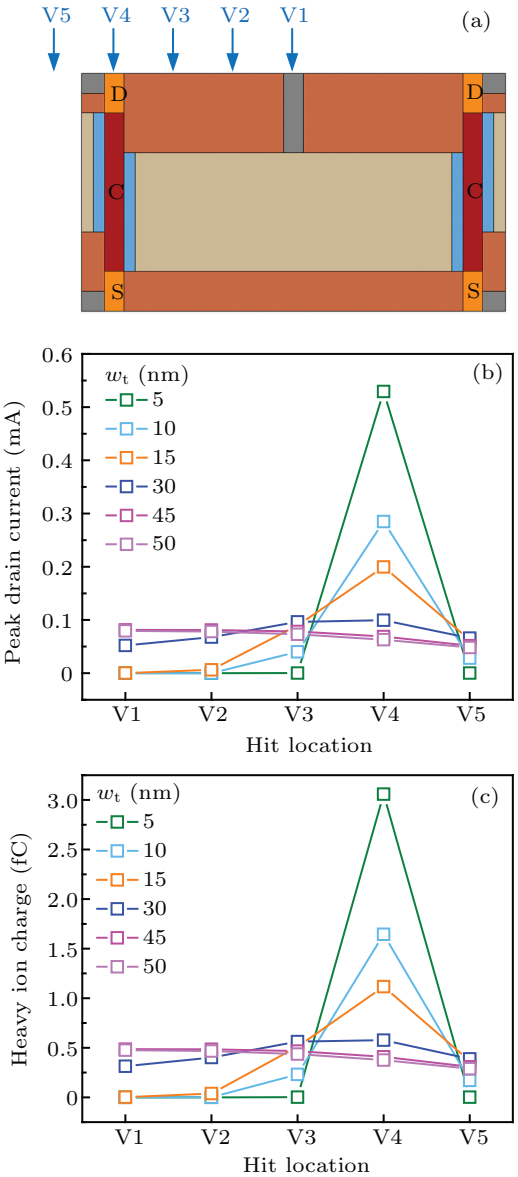


Fig. 11. (a) The ion strikes EHBNT-TFET in location V1 to V5 from vertical direction. (b) Peak drain current and (c) heavy ion-generated charge for vertical ion hit locations under on-state with various w_t, LET = 10 MeV·cm^2/mg.

The SET response at diverse horizontal hit locations with various w_t is evaluated in Fig. 12. When w_t is larger than 5 nm, peak drain current is found to increase firstly when hit location moves from drain (H1) to channel (H3) and then drops until hit location arrives at source (H5). When w_t equals to 5 nm, I_{d_peak} has the maximum at H2. Besides, as w_t increases, I_{d_peak} increases firstly and then declines when the ion strikes at H1/H5, which decreases monotonously at hit location near channel (H2/H3/H4). As presented in Fig. 12(b), when hit location is away from the center of channel, heavy ion-generated charge in silicon nanotube decreases gradually. Heavy ion-generated charge reaches a maximum and more carriers are generated at hit location H3. In addition, we found that $Q_{heavyion}$ when the ion striking at H1 is exactly the same with that at H5, the corresponding I_{d_peak} is not equal. The $Q_{heavyion}$ and I_{d_peak} when the ion strikes at H2 and H4 is also the same situation. Due to the small ion track region at $w_t = 5$ nm, $Q_{heavyion}$ striking at H3 is the same with that at H2/H4. Compared with I_{d_peak} at hit location near source, I_{d_peak} at hit location close to drain is clearly larger owing to the short collection path of generated electron, which is consistent with above analysis of the effect of angle on SET current.

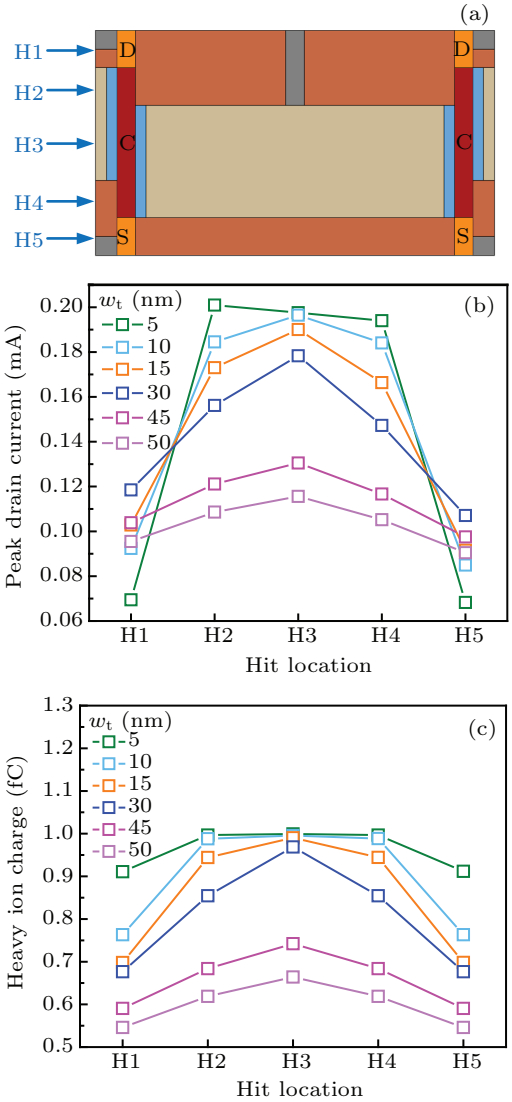


Fig. 12. (a) The ion strikes EHBNT-TFET in location H1 to H5 from horizontal direction. (b) Peak drain current and (c) heavy ion-generated charge for horizontal ion hit locations under on-state with various w_t, LET = 10 MeV·cm^2/mg.

In addition, abundant EHPs are generated in drain/source when the ion with low w_t strikes at H1/H5, and the recombination rate increases due to the low electric field. As a result, I_{d_peak} declines when w_t decreases from 30 nm to 5 nm, although $Q_{heavyion}$ is increasing. When the ion strikes at H2/H3/H4, EHPs are mainly generated in the channel with high electric field, so that the electrons and holes are separated quickly. Therefore, the changing of w_t results in little impact on recombination rate. I_{d_peak} is found to decrease with w_t increasing only under the effect of declined $Q_{heavyion}$.

According to the analysis above, the most sensitive hit location strongly depends on w_t. For ion striking from vertical direction, incidence from channel (V4) has a severe SET response in EHBNT-TFET until w_t exceeds 30 nm. The most sensitive region to SET effect is the center position (V1) under large w_t. For the ion striking from horizontal direction, the most sensitive region is the center position (H3) when w_t is larger than 5 nm, which is H2 at $w_t = 5$ nm.

4. Conclusion

In this paper, the SET effect in EHBNT-TFET has been carried out with 3-D TCAD simulations. Subjected to heavy ion irradiation, EHBNT-TFET suffers a serious SET effect. For the ion with characteristic radius of 50 nm and LET of 10 MeV·cm^2/mg, the peak drain current reaches up to 0.08 mA, which is much larger than on-state current. As LET enlarges from 2 MeV·cm^2/mg to 10 MeV·cm^2/mg, the peak drain current increases monotonically from 0.015 mA to 0.08 mA, and the corresponding Q_{coll} rises up from 0.082 fC to 0.413 fC. For the variation of characteristic radius, the transient current reaches a maximum at at $w_t = 45$ nm. The strike angle shows an greater impact on peak drain current especially for the smaller w_t. As w_t increases, the strike angle corresponding to the maximum of I_{d_peak} increases from 45° to 56° and then remains unchanged. The I_{d_peak} increases 0.014 mA and Q_{coll} increases 0.06 fC as the drain bias ranges from 0.1 V to 0.9 V, while the outer-gate bias is found to present an opposite tendency and less influence. When the ion strikes from the vertical and horizontal directions, the hit location sensitivity strongly depends on w_t, which is affected by heavy ion-generated charge, collection distance of electron and electric filed. This provides guidance for future research on the antiradiation application of TFET-based devices.

Acknowledgements

Project supported in part by the National Natural Science Foundation of China (Grant No. 61974056), the Natural Science Foundation of Shanghai (Grant No. 19ZR1471300), Shanghai Science and Technology Innovation Action Plan (Grant No. 19511131900), and Shanghai Science and Technology Explorer Plan (Grant No. 21TS1401700).

References

[1] Taur Y 2002 *IBM J. Res. Dev.* **46** 213
[2] Seabaugh A C and Zhang Q 2010 *Proc. IEEE* **98** 2095
[3] Asra R, Shrivastava M, Murali K V R M, Pandey R K, Gossner H and Rao V R 2011 *IEEE Trans. Electron Dev.* **58** 1855
[4] Datta S, Liu H and Narayanan V 2014 *Microelectron. Reliab.* **54** 861
[5] Raushan M A, Alam N and Siddiqui M J 2018 *IEEE Trans. Electron. Dev.* **65** 4701
[6] Boucart K and Ionescu A M 2007 *IEEE Trans. Electron Dev.* **54** 1725
[7] Kim S W, Kim H W, Liu T J K, Choi W Y and Park B G 2016 *IEEE Trans. Electron. Dev.* **63** 1774
[8] Seo J H, Yoon Y J, Lee S, Lee J H, Cho S and Kang I M 2015 *Curr. Appl. Phys.* **15** 208
[9] Musalgaonkar G, Sahay S, Saxena R S and Kumar M J 2019 *IEEE Trans. Electron. Dev.* **66** 2809
[10] Lattanzio L, Michielis L D and Ionescu A M 2012 *Solid State Electron.* **74** 85
[11] Wang X, Sun Y, Liu Z, Liu Y, Li X and Shi Y 2022 *Silicon* **14** 9071
[12] Qin J, Chen S, Liu B, Liu Z, Liang B and Du Y 2011 *Chin. Phys. B* **20** 129401
[13] Moreno E G, Picos R, Isern E, Roca M, Bota S and Suenaga K 2009 *IEEE Trans. Nucl. Sci.* **56** 2910
[14] Dodd P E, Shaneyfelt M R, Schwank J R and Felix J A 2010 *IEEE Trans. Nucl. Sci.* **57** 1747
[15] Kim J, Lee J S, Han J W and Meyyappan M 2018 *IEEE Electron. Dev. Lett.* **39** 1840
[16] Kaushal G, Rathod S S, Maheshwaram S, Manhas S K, Saxena A K and Dasgupta S 2012 *IEEE Trans. Electron. Dev.* **59** 1563
[17] Munteanu D 2008 *IEEE Trans. Nucl. Sci.* **55** 1854
[18] Li D, Liu T, Zhao P, Wu Z, Wang T and Liu J 2022 *Chin. Phys. B* **31** 056106
[19] Manohari R G, Nagarajan K K and Srinivasan R 2017 *Int. Conf. On Nextgen Electronic Technologies: Silicon to Software*, Mar. 23–25, 2017, Chennai, India, p. 172
[20] Wu Y and Takahashi Y 2017 *ECS Meeting Abstracts* **2** 1143
[21] Wang Q, Liu H, Wang S and Chen S 2018 *IEEE Trans. Nucl. Sci.* **65** 2250
[22] Chong C, Liu H, Wang S, Chen S and Xie H 2021 *Micromachines* **12** 609
[23] Synopsys Inc. 2018 *Sentaurus Device User Guide*
[24] Fahad H M and Hussain M M 2013 *IEEE Trans. Electron. Dev.* **60** 1034
[25] Sun Y, Shao J, Liu Z, Li X, Liu Y and Shi Y 2021 *IEEE Trans. Electron. Dev.* **68** 6001
[26] Tian G, Bi J, Xu G, Xi K, Yang X, Yin H, Xu Q and Wang W 2020 *Semicond. Sci. Technol.* **35** 105010
[27] Liu H, Cotter M, Datta S and Narayanan V 2014 *IEEE Trans. Device Mater. Reliab.* **14** 732
[28] Liu Z, Chen S, Chen J, Qin J and Liu R 2012 *Chin. Phys. B* **21** 099401